

pubs.acs.org/JPCL Letter

# Ultrafast Exciton Dynamics of CH<sub>3</sub>NH<sub>3</sub>PbBr<sub>3</sub> Perovskite Nanoclusters

Vivien L. Cherrette, Kai-Chun Chou, David Zeitz, Melissa Guarino-Hotz, Mariam Khvichia, Jeremey Barnett, Allison Win, Finn Babbe, and Jin Z. Zhang\*



Cite This: J. Phys. Chem. Lett. 2024, 15, 5177-5182



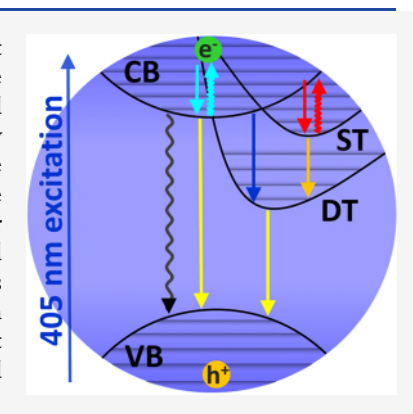
**ACCESS** I

III Metrics & More

Article Recommendations

Supporting Information

**ABSTRACT:** Exciton dynamics of perovskite nanoclusters has been investigated for the first time using femtosecond transient absorption (TA) and time-resolved photoluminescence (TRPL) spectroscopy. The TA results show two photoinduced absorption signals at 420 and 461 nm and a photoinduced bleach (PB) signal at 448 nm. The analysis of the PB recovery kinetic decay and kinetic model uncovered multiple processes contributing to electron—hole recombination. The fast component ( $\sim$ 8 ps) is attributed to vibrational relaxation within the initial excited state, and the medium component ( $\sim$ 60 ps) is attributed to shallow carrier trapping. The slow component is attributed to deep carrier trapping from the initial conduction band edge ( $\sim$ 666 ps) and the shallow trap state ( $\sim$ 40 ps). The TRPL reveals longer time dynamics, with modeled lifetimes of 6.6 and 93 ns attributed to recombination through the deep trap state and direct band edge recombination, respectively. The significant role of exciton trapping processes in the dynamics indicates that these highly confined nanoclusters have defect-rich surfaces.



Perovskite nanoclusters (PNCLs) are a class of ultrasmall quasi-crystalline semiconductor nanoparticles with strong quantum confinement and a single size or narrow size distribution. They are ligand passivated and exhibit the ABX<sub>3</sub> perovskite structure (A being a monovalent cation, B being a metal divalent cation, and X being a halide anion) and some have been shown to exhibit layered, disc-like structures in comparison to the characteristic cubic structures of PQDs. PNCLs are intermediates and building blocks for larger perovskite quantum dots (PQDs) or nanocrystals. Investigating PNCLs can shed light on the growth mechanisms of PQDs on a molecular and atomic level and assist in the rational design of high-quality PQDs with molecular precision.

Recent studies have found that the CH<sub>3</sub>NH<sub>3</sub>PbBr<sub>3</sub> PNCL system forms a distorted orthorhombic structure.<sup>3</sup> Similar to PQDs, PNCLs are expected to exhibit quantum confinement effects due to their close proximity in size to the Bohr radius of CH<sub>3</sub>NH<sub>3</sub>PbBr<sub>3</sub> perovskites, ~2.0 nm.<sup>4</sup> However, PNCLs are much smaller and exhibit an energetically blue-shifted, characteristic absorption peak around 450 nm, compared to PQDs, which have a characteristic broad absorption band with an onset around 520 nm.<sup>5</sup> The absorption band of PNCLs indicates a narrower size distribution in comparison with more polydisperse PQDs. The polydispersity of PQDs after synthesis is due to a mixture of these PNCLs and other synthetic intermediate clusters.

Another related intermediate cluster known as metal halide molecular clusters (MHMCs) can form during the PNCL and PQD synthesis. Ligand-passivated MHMCs lack the A component in perovskite yet still form octahedrally coordinated Pb–Br polyhedral structures similar to the PbBr<sub>6</sub>

octahedra formed in perovskite.<sup>6</sup> The PNCLs are likely formed from the MHMC intermediates and may retain some of the MHMC optical characteristics. Although much work has been done optimizing synthesis and characterizing the optical and structural properties of PNCLs, there has yet to be a kinetic study on their exciton dynamics.<sup>1–3</sup>

Studying the exciton dynamics will give us insight into the role defects play in the optoelectronic properties of these novel nanoclusters. For instance, internal or surface defects strongly affect the photoluminescence quantum yield (PLQY). Defects are often significant in nanocrystals compared to bulk materials due to their large surface to volume ratio. In smaller PQDs, incomplete surface passivation due to steric hindrance of the ligands can introduce more surface defects. From a kinetics perspective, the high density of surface defect states can contribute to trapping and nonradiative recombination of excitons, thereby lowering the PLQY. PNCLs have a much larger surface to volume ratio than their PQD counterparts, making them a suitable model system for studying the effects of surfaces or interfaces on exciton dynamics.

Surface defects are known to generate trap states within the band gap, which allow for alternate radiative and nonradiative exciton recombination pathways. Shallow trap states, located near the band edges, coupled with low phonon energies lead to

 Received:
 April 24, 2024

 Revised:
 May 2, 2024

 Accepted:
 May 3, 2024



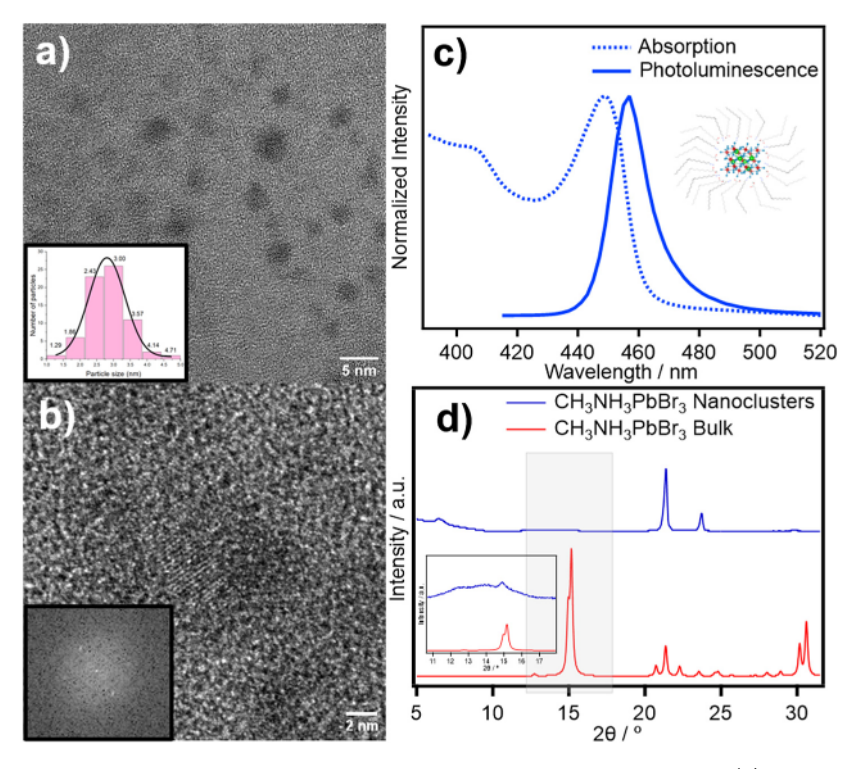


**Figure 1.** (a) HR-TEM of PNCLs showing monodispersed particle size with a histogram in the inset, (b) HR-TEM of single PNCL showing distorted orthorhombic crystal structure and fast Fourier transform (inset), and (c) absorption and photoluminescence spectra of CH<sub>3</sub>NH<sub>3</sub>PbBr<sub>3</sub> PNCLs suspended in toluene. Spectra are overlaid and normalized to the corresponding peak absorption and emission. The inset shows the orthorhombic structure of CH<sub>3</sub>NH<sub>3</sub>PbBr<sub>3</sub> PNCLs composed of CH<sub>3</sub>NH<sub>3</sub>+ (green); Pb<sup>2+</sup> (red); and Br<sup>-</sup> (blue) passivated with oleic acid and oleylamine ligands (structure constructed using VESTA (COD ID: 4510745)). <sup>11</sup> (d) X-ray diffraction (XRD) patterns of CH<sub>3</sub>NH<sub>3</sub>PbBr<sub>3</sub> PNCLs with theoretical orthorhombic powder patterns calculated in VESTA (ICSD: 158306). <sup>12</sup>

low nonradiative recombination rates and thus long carrier lifetimes. This manifests as a broadening of the steady-state optical absorption and emission spectra. Deep trap states, located near the middle of the bandgap, generate nonradiative recombination pathways that can significantly reduce PLQY due to multiphonon recombination processes. 10

Herein, this study utilizes femtosecond transient absorption spectroscopy (TA) and time-resolved photoluminescence (TRPL) to probe the exciton properties of PNCLs. The results help to clarify the key kinetic processes involved in the exciton dynamics of the PNCL.

Hot ligand assisted reprecipitation was used to synthesize stable PNCL suspensions in toluene.<sup>5</sup> This synthetic method at elevated temperatures was selected because room-temperature synthesis typically shows signs of degradation after several days. PNCLs synthesized at elevated temperatures are stable for about a week under ambient conditions, which is necessary for laser operation to conduct the exciton dynamics studies.

High resolution electron microscopy (HR-TEM) displayed in Figure 1a indicates a relatively monodisperse size distribution. The Figure 1a inset displays a size distribution histogram where the nanoclusters have an average diameter of  $2.8 \pm 0.5$  nm with a 22% root mean squared. Figure 1b shows a single PNCL with the fast Fourier transform in the inset. There is some uncertainty associated with the HR-TEM results due to PNCLs instability as a solid. PNCLs tend to aggregate and create larger PQDs when dried to a solid. To avoid this aggregation for powder X-ray diffraction (XRD) measurements, the PNCLs were suspended and stabilized in paraffin as previously reported in literature. Figure 1d shows the powder

XRD with the theoretical orthorhombic CH<sub>3</sub>NH<sub>3</sub>PbBr<sub>3</sub> patterns. The HR-TEM shows a d-spacing of  $\sim 0.6$  nm, which agrees with the theoretical CH<sub>3</sub>NH<sub>3</sub>PbBr<sub>3</sub> 14.9° XRD peak. The PXRD shows a broad 14.9° peak, the lack of the 15.1° peak associated with the (101) reflection, and the introduction of the broad 12.5° and 13.9° peaks. The peaks at 21.4° and 23.7° are from the stabilizing paraffin medium and capping ligand. This result shows that PNCLs have a distorted orthorhombic structure and agrees with previously reported HR-TEM and XRD.<sup>3</sup>

Figure 1c shows the normalized absorption and steady-state photoluminescence (PL) of the PNCL suspensions. The Figure 1c inset illustrates the orthorhombic structured PNCL with oleic acid and oleylamine passivating ligands. The UV—vis absorption spectrum exhibits an excitonic absorption peak at 449 nm, while the PL spectrum shows a single emission peak at 457 nm with a full-width at half-maximum (FWHM) of 19 nm. The PNCLs have a relatively large Stokes shift of 8 nm in comparison to the traditional PQDs that usually have a negligible Stokes shift. A larger Stokes shift has been observed in more confined structures and attributed to a confined hole state associated with defects. <sup>13</sup>

The steady-state UV—vis absorption and PL spectra show strong absorption and emission bands that are substantially blue-shifted compared to that of corresponding PQDs, indicating strong quantum confinement due to their small size. The single, narrow absorption band and narrow FWHM of the PL band are characteristic of PNCLs due to their narrow size distribution. Figure S1 shows the PL spectrum best fits with a double Gaussian function, with fitting parameters summarized in Table S1. The inhomogeneous broadening

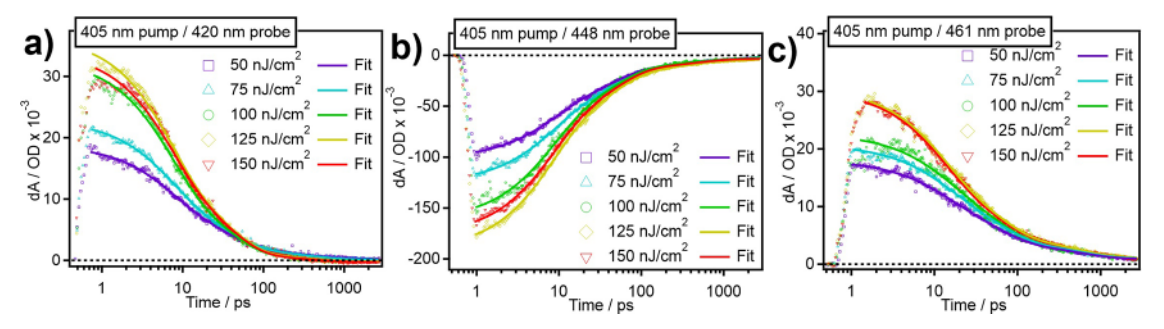


Figure 2. Power dependent kinetic decay profiles of PNCLs excited with 405 nm at different probe signals: (a) 420 nm probe (PA<sub>1</sub>), (b) 448 nm probe (PB), and (c) 461 nm probe (PA<sub>2</sub>). Probe signals are single wavelengths with the highest dA intensity in the difference in the absorption spectrum in Figure 3a.

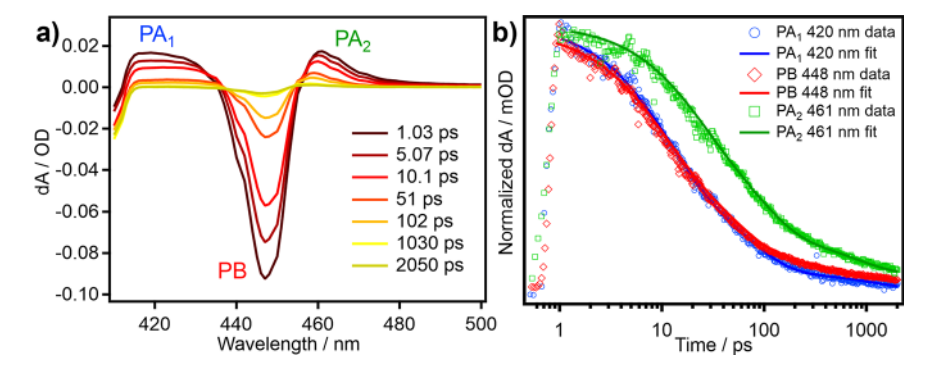


Figure 3. (a) Difference in absorption spectrum as a function of wavelength and varying probe delay times and (b) overlaid kinetic decay profiles and fits of the PA<sub>1</sub>, PB, and PA<sub>2</sub> signals.

observed in the PL suggests the possibilities of two different particle size populations, the presence of defects, or phonon broadening. 14 The PL excitation (PLE) spectrum in Figure S2 was taken at the peak locations in the fitted PL spectrum (456 and 465 nm). Both wavelength results show the same spectrum, indicating that both emissions originate from the same peak at 447 nm, which agrees with the first excitonic absorption. There is a small shoulder at 405 nm, which suggests the presence of a second excited state. Furthermore, Figure S3 shows wavelength-dependent TRPL with 405 nm excitation on the two fitted PL peak locations, with the singlewavelength fitting parameters shown in Table S2. There were no changes in the kinetics, indicating that the PL band originates from the same particle population. Thus, the inhomogeneous broadening may indicate the presence of defects or phonon broadening.

Femtosecond TA studies of PNCLs were performed with excitation above the band edge (405 nm) or near the band edge (425 nm) and probed with a broadband white light continuum as a function of the time delay between the pump and probe pulses. Although closer to the band edge, the samples excited at 425 nm showed a lower signal-to-noise (S/N) ratio due to the inference between the pump and probe light. Because of this, further TA studies were carried out using an above-band-edge excitation at 405 nm. Since the 405 nm excitation is higher in energy than 425 nm, hot electrons are more likely generated with the 405 nm excitation, which may contribute to longer time decays on the ultrafast time scale.

Figure S4 and Table S3 show the kinetic comparison and fit parameters of the 450 nm bleach recovery between the 405 and 425 nm excitation with a similar low power. There is good agreement between 405 and 425 nm results in longer time scales. However, there were some slight differences on the

shorter time scales (<10 ps). From the raw fit of the bleach recovery, the 405 nm data showed a fast time component of 7.6 ps, while the 425 nm data showed a slightly shorter 7 ps time constant. Based on the UV—vis spectrum, the 405 nm excitation is exciting a higher energy electronic band or state; thus, the difference could also be due to internal electronic conversion from this higher excited state to the first excited state. In addition, MHMCs do happen to have an absorption band peaked around 405 nm; however, the UV—vis spectrum shows that this band is weak compared to the absorption of the PNCLs and their contribution to the TA/TB signal is expected to be small or negligible compared to that of PNCLs. On balance, since the 405 nm data are overall quite similar to the 425 nm data and have a better S/N ratio, the rest of the study focuses on the 405 nm excitation data.

As observed in analogous PQDs, TA analysis can be challenging due to overlapping signals from photoinduced absorption (PA) signals, hot carrier cooling, and stimulated emission, especially at high excitation powers. <sup>8,15,16</sup> In addition, nonlinear processes like Auger recombination and/or exciton—exciton annihilation can also overlap with the signal. <sup>8,17</sup> Thus, power dependent studies were carried out with the goal of finding the threshold excitation power below which nonlinear processes have no effect.

Figure 2a—c shows the kinetic decay profile at different powers for each photoinduced signal. To identify the threshold power, the PNCL sample was pumped with several pulse energies: 50, 75, 100, 125, and 150 nJ/cm². The photoinduced transient signals, or monitored wavelengths at maximum intensity, were determined from the difference in the absorption spectrum plotted in Figure 3a. There are two photoinduced absorption features labeled as PA<sub>1</sub> and PA<sub>2</sub> for the peak positions at 420 and 461 nm, and a photoinduced

bleach signal (labeled PB) peaked at 448 nm. Each singlewavelength probe signal was normalized and best fitted with a triple exponential function to determine the decay time constants ( $\tau_x$ , in ps) and relative amplitudes ( $A_x$ , %), where x is the corresponding fitted exponential decay. The corresponding fitting parameters and average decay times for the PA/PB signals are reported in Table S4. The calculated average decay times of the three probe signals, PA1, PB, and PA<sub>2</sub>, were calculated using Equation S2. The respective time constants of each PA or PB feature remained consistent over the different excitation powers used, suggesting invariable kinetics within the 50-150 nJ/cm<sup>2</sup> excitation range. As observed in smaller PQD systems, highly confined excitons within a single particle limit direct band edge recombination, resulting in power-independent decay dynamics. 7,18 This phenomenon is likely occurring in PNCLs which are smaller and more confined and may absorb fewer photons per pulse in comparison to larger nanoparticles like PQDs. However, further analysis of the amplitude evolution of each signal as a function of power in Figure S5 shows that the PA and PB features have more nonlinearity in powers above 100 nJ/cm<sup>2</sup>. The nonlinearity suggests nonlinear effects such as excitonexciton annihilation or Auger recombination become more dominant.8,17 To avoid these nonlinear kinetics and/or an excitation bottleneck, the data from the 50 nJ/cm<sup>2</sup> excitation was used for the exciton dynamic study and kinetic model.

The 420 nm PA<sub>1</sub> decay profile can be fit with a triple exponential with fast, medium, and slow time constants of 6.6  $\pm$  0.5, 36  $\pm$  5, and 370  $\pm$  50 ps. The PB signal can be fit with similar time constants. Figure 3b shows the overlaid PA<sub>1</sub>, PB, and PA2 kinetic decays to confirm the kinetic agreement. In addition, Figure S6 shows box plots comparing the fast, medium, and slow time constants of each corresponding TA signal. The similar kinetics of the PA1 and PB signals suggest that they are associated with the same dynamics and processes. The initial positive absorption feature of PA<sub>1</sub> is attributed to electrons excited to the first excitonic state or conduction band (CB). The PA<sub>1</sub> decay profile reflects the dynamics of the photogenerated electrons populating the CB. The PB reflects recovery of the electrons back in the valence band (VB), which matches the dynamics of the PA<sub>1</sub>. The 461 nm PA<sub>2</sub> feature shows longer kinetics compared to the PB or PA<sub>1</sub>. The PA<sub>2</sub> kinetics shows fast, medium, and slow time constants of 11.3  $\pm$ 0.8, 55  $\pm$  4, and 580  $\pm$  70 ps. The overlaid kinetic decay profiles in Figure 3b and the time constant comparisons in Figure S6 show that the PA<sub>2</sub> feature has a slow decay unique to the PNCLs. This slower decay may be attributed to trap states absorbing the 461 nm probe.

The 448 nm PB decay profile is attributed to the repopulation of ground state electrons due to good agreement with the first excitonic absorption in the UV–vis spectrum shown in Figure 1c. The PB decay profile was best fit to a triple exponential with fast  $(7.6 \pm 0.5 \text{ ps})$ , medium  $(43 \pm 3 \text{ ps})$ , and slow  $(450 \pm 40 \text{ ps})$  decay time constants. The decay profile was normalized to obtain the relative amplitudes as percentages of each decay time component. Relative amplitudes were used to indicate the dominant processes contributing to the bleach recovery. The fast and medium time components have large amplitudes,  $46 \pm 1\%$  for  $A_1$  and  $40 \pm 1\%$  for  $A_2$ , suggesting that these are the dominant processes occurring in bleach recovery. The slow time component has an amplitude of  $10.4 \pm 0.5\%$   $(A_3)$  indicating a minor process contributing to bleach recovery. Although the PB decay profile

provides information on ultrafast recombination kinetics, it is an incomplete picture of the kinetics on longer time scales because the PB signal was not fully recovered within the time window (2480 ps). Therefore, TRPL was done to map out the long-time scale recombination kinetics to the nanosecond regime.

Figure 4 shows the PL decay profile of PNCLs excited at 405 nm, with emission monitored at 454 nm. The PL decay

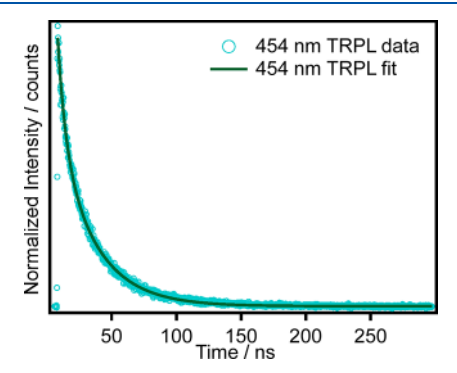


Figure 4. Time-resolved photoluminescence of PNCLs excited at 405 nm and the emission monitored at  $\lambda_{\rm max}$ = 454 nm.

was best fit to a double exponential function, and the fitting parameters and average PL decay time are reported in Table S5. The PL decay profile of the PNCLs revealed a fast  $(6.0 \pm 0.2 \text{ ns})$  and slow  $(28.6 \pm 0.2 \text{ ps})$  decay time constant. The average PL decay lifetime was calculated, using Equation S2, to be 26 ps.

The fast and slow components have relative amplitudes of  $33.8 \pm 0.5\%$  and  $61.0 \pm 0.5\%$ , suggesting the competitive nature of the two processes contributing to the observed PL. This indicates the presence of a trap state within the bandgap that facilitates radiative recombination. The fast 6 ns component was contributed to electron—hole recombination through a trap state and the slow 28.6 ns component is consistent with direct band edge recombination.<sup>7</sup> A power dependent study was performed to determine the saturation of the trap states in Figure S7. However, there is no trend in the power dependence, and the kinetics are unchanging. The lack of power dependence in the TRPL results could be due to a high density of trap states or the pump power not being high enough to trigger trap saturation.

Radiative and nonradiative recombination lifetimes were found using TRPL and relative PLQY (28%) to determine dominant decay processes. The PLQY provides a measure of the radiative versus nonradiative processes. The relationship between observed PL lifetime ( $\tau_{\rm obs}$ ), radiative lifetime ( $\tau_{\rm r}$ ), and PLQY is shown in eq 1. <sup>19</sup>

$$\tau_{\rm r} = \frac{\tau_{\rm obs}}{\rm PLQY} \tag{1}$$

The radiative and nonradiative lifetimes were calculated using eq 2, 19

$$\frac{1}{\tau_{\rm obs}} = \frac{1}{\tau_{\rm r}} + \frac{1}{\tau_{\rm nr}} \tag{2}$$

where  $(\tau_{\rm obs})$ ,  $(\tau_{\rm r})$ , and  $(\tau_{\rm nr})$  are the observed average PL lifetime, radiative lifetime, and nonradiative lifetime. Using the average observed lifetime (26 ns) and measured PLQY (28%) of PNCLs,  $\tau_{\rm r}$  and  $\tau_{\rm nr}$  were calculated to be 93 and 37 ns,

respectively. The radiative lifetime is over twice that of the nonradiative lifetime, indicating the dynamics are dominated by nonradiative processes. Unlike PQD samples where radiative processes are dominant, PNCLs are similar to MHMC samples, where nonradiative processes are dominant. The low PLQY and dominant nonradiative lifetime suggest the presence of defect-related recombination and/or deep trap states facilitating multiphonon emission.

The TA and TRPL results were used to construct a kinetic model and propose possible recombination processes occurring in PNCLs. Figure S8 shows the overlaid TA and TRPL kinetic decay profiles and a full kinetic fit to confirm the decay lifetimes. Kinetic modeling using the full decay profile from the experimental TA and TRPL data were used to construct a simple mechanism to aid in explaining the possible relaxation processes involved in these novel clusters. Details of the kinetic modeling are available in the Supporting Information: Figures S9–S11, Table S6, and Equations S3–S7.

Figure 5 shows a proposed kinetic model for the exciton dynamics of PNCLs with a focus on key processes under low

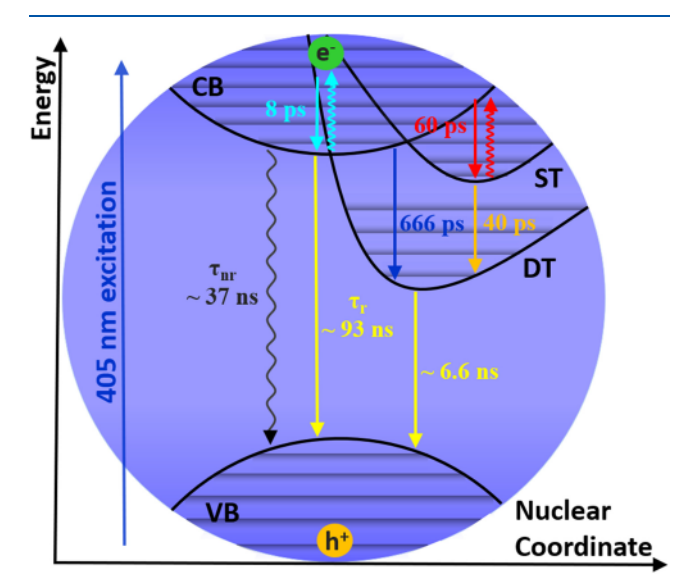


**Figure 5.** Kinetic model of a PNCL. The lifetimes of each state were calculated using the kinetic model of the TA and TRPL results.

excitation power. The proposed exciton processes involve the CB, CB edge ( $\mathrm{CB}_{\mathrm{edge}}$ ), shallow trap (ST) states, deep trap (DT) states, and VB. An exciton is generated after excitation with an energy above the band gap (405 nm). Exciting above the band edge provides excess kinetic energy, and therefore, the electron will relax to the  $\mathrm{CB}_{\mathrm{edge}}$  through electron—phonon interactions. <sup>16</sup>

The fast component ( $\sim$ 8 ps) in the PB decay profile was attributed to vibrational relaxation or cooling of the excitons within the CB. In MHMC systems, vibrational relaxation has a similar ultrafast decay lifetime of  $\sim$ 7 ps, which suggests that PNCLs have some MHMC character. After the electrons have relaxed to the CB<sub>edge</sub>, they can go through multiple pathways, including trapping into trap states. The Urbach absorption tail seen in PNCLs, also seen in semiconductor nanocrystals, is known to be due to localized energy states (shallow trap/defect sites) near the band-edge arising from the structural disorder or lattice defects. In the simplified model, it was found that the PB medium component ( $\sim$ 60 ps) was attributed to shallow trapping below the CB<sub>edge</sub>. It was also

found that the CB and ST states were coupled to a DT state (40 and 666 ps), and both forward processes were contributing to deep trapping. From the kinetic model, these processes compete and contribute to the overall slow time constant in the PB ( $\sim$ 450 ps).

In addition, the triple exponential decay of the PB signal indicates that the dynamic processes are not simple sequential or parallel processes but also include reverse processes. 7,23 The possible reverse processes are shown in Figure 5 as upward curved arrows. The reverse processes are usually expected to be slower than the forward process.<sup>7</sup> The reverse process is likely due to back energy transfer from a vibrationally relaxed state, like the  $\ensuremath{\mathsf{CB}_{\mathsf{edge}}}$  or ST and DT states, to higher vibrational states, resulting in multiexponential character. The respective rate constants and associated time constants are listed in Table S6. In the kinetic model, multiple combinations of rate constants and time constants were simulated to evaluate the most plausible processes occurring within the PNCL system. Although the PB signal uncovers critical kinetic processes, these processes did not contribute to overall observed PL lifetime.

In PNCLs, the relaxed electron can recombine radiatively with a 93 ns lifetime and nonradiatively with a 37 ns lifetime. Although direct band edge recombination dominates, the electrons may also recombine through deep trapping. The fast decay lifetime ( $\sim$ 6 ns) in the TRPL agrees well with the kinetic model ( $\sim$ 6.6 ns) and is attributed to recombination through the DT state.

In summary, the exciton dynamics of methylammonium lead halide PNCLs have been investigated for the first time using femtosecond TA spectroscopy and TRPL. The fast and medium components in the PB kinetics were found to be the dominant processes, indicating that vibrational relaxation in the excited state and shallow trapping play a significant role in recombination. The deep trap state provides an alternate pathway for recombination that is competitive with direct band edge recombination seen in the observed PL. However, due to the relatively low PLQY, fast nonradiative lifetime, longer PA $_2$  time decay, and evidence of exciton trapping, there is likely a high density of trap states in PNCLs suggesting that they have defect-rich surfaces. The surface defects in PNCLs may be causing exciton trapping and contribute to overall shorter lifetimes, in comparison to PQDs.

#### ASSOCIATED CONTENT

# Supporting Information

The Supporting Information is available free of charge at https://pubs.acs.org/doi/10.1021/acs.jpclett.4c01203.

Experimental section, Fitting Parameters, and additional plotted data and figures (PDF)

## AUTHOR INFORMATION

### **Corresponding Author**

Jin Z. Zhang — Department of Chemistry and Biochemistry, University of California, Santa Cruz, California 95064, United States; o orcid.org/0000-0003-3437-912X; Email: zhang@ucsc.edu

# **Authors**

Vivien L. Cherrette – Department of Chemistry and Biochemistry, University of California, Santa Cruz, California 95064, United States

- Kai-Chun Chou Department of Chemistry and Biochemistry, University of California, Santa Cruz, California 95064, United States; orcid.org/0000-0002-0282-3604
- David Zeitz Department of Chemistry and Biochemistry, University of California, Santa Cruz, California 95064, United States
- Melissa Guarino-Hotz Department of Chemistry and Biochemistry, University of California, Santa Cruz, California 95064, United States; orcid.org/0000-0001-6310-8156
- Mariam Khvichia Department of Chemistry and Biochemistry, University of California, Santa Cruz, California 95064, United States
- Jeremey Barnett Department of Chemistry and Biochemistry, University of California, Santa Cruz, California 95064, United States
- Allison Win Department of Chemistry and Biochemistry, University of California, Santa Cruz, California 95064, United States; orcid.org/0000-0001-7867-1953
- Finn Babbe Chemical Science Division, Lawrence Berkeley National Laboratory, Berkeley, California 94720, United States; © orcid.org/0000-0002-9131-638X

Complete contact information is available at: https://pubs.acs.org/10.1021/acs.jpclett.4c01203

#### **Notes**

The authors declare no competing financial interest.

#### ACKNOWLEDGMENTS

VLC is grateful to the Chemical Science Division at Lawrence Berkeley National Laboratory (LBNL) for the use of their B30 facilities. Zhang lab at UCSC is grateful to the US NSF for financial support under Award Numbers CHE-1904547 and CHE-2203633. FB acknowledges support from the U.S. Department of Energy, Office of Science, Office of Basic Energy Sciences, Fuels from Sunlight Hub under Award Number DE-SC0021266. We would like to acknowledge the Molecular Foundry National Center of Electron Microscopy (NCEM) at LBNL for the HR-TEM. Work at the Molecular Foundry was supported by the Office of Science, Office of Basic Energy Sciences, of the U.S. Department of Energy under Contract No. DE-AC02-05CH11231.

#### REFERENCES

- (1) Vickers, E. T.; Chen, Z.; Cherrette, V.; Smart, T.; Zhang, P.; Ping, Y.; Zhang, J. Z. Interplay between Perovskite Magic-Sized Clusters and Amino Lead Halide Molecular Clusters. *Research* **2021**, 2021, 6047971.
- (2) Zhang, B.; Altamura, D.; Caliandro, R.; Giannini, C.; Peng, L.; De Trizio, L.; Manna, L. Stable CsPbBr<sub>3</sub> Nanoclusters Feature a Disklike Shape and a Distorted Orthorhombic Structure. *J. Am. Chem. Soc.* **2022**, *144* (11), 5059–5066.
- (3) Guarino-Hotz, M.; Barnett, J. L.; Chou, K.-C.; Win, A. A.; Zhang, H.; Song, C.; Oliver, S. R. J.; Zhang, J. Z. Structural Study of Paraffin-Stabilized Methylammonium Lead Bromide Magic-Sized Clusters. *J. Phys. Chem. C* **2023**, *127* (6), 3367–3376.
- (4) Tanaka, K.; Takahashi, T.; Ban, T.; Kondo, T.; Uchida, K.; Miura, N. Comparative Study on the Excitons in Lead-Halide-Based Perovskite-Type Crystals CH<sub>3</sub>NH<sub>3</sub>PbBr<sub>3</sub> CH<sub>3</sub>NH<sub>3</sub>PbI<sub>3</sub>. Solid State Commun. 2003, 127 (9–10), 619–623.
- (5) Guarino-Hotz, M.; Barnett, J. L.; Pham, L. B.; Win, A. A.; Cherrette, V. L.; Zhang, J. Z. Tuning between Methylammonium Lead Bromide Perovskite Magic-Sized Clusters and Quantum Dots

- through Ligand Assisted Reprecipitation at Elevated Temperatures. J. Phys. Chem. C 2022, 126 (32), 13854–13862.
- (6) Zhang, H.; Vickers, E. T.; Erickson, S.; Guarino-Hotz, M.; Barnett, J. L.; Ghosh, S.; Zhang, J. Z. Synthesis and Properties of Stable Amino Metal Halide Molecular Clusters in the Solid State. *J. Phys. Chem. Lett.* **2022**, *13* (45), 10543–10549.
- (7) Naghadeh, S. B.; Luo, B.; Pu, Y.-C.; Schwartz, Z.; Hollingsworth, W. R.; Lindley, S. A.; Brewer, A. S.; Ayzner, A. L.; Zhang, J. Z. Size Dependence of Charge Carrier Dynamics in Organometal Halide Perovskite Nanocrystals: Deciphering Radiative Versus Nonradiative Components. *J. Phys. Chem. C* **2019**, *123* (7), 4610–4619.
- (8) Luo, B.; Pu, Y.-C.; Yang, Y.; Lindley, S. A.; Abdelmageed, G.; Ashry, H.; Li, Y.; Li, X.; Zhang, J. Z. Synthesis, Optical Properties, and Exciton Dynamics of Organolead Bromide Perovskite Nanocrystals. *J. Phys. Chem. C* **2015**, *119* (47), 26672–26682.
- (9) Kirchartz, T.; Markvart, T.; Rau, U.; Egger, D. A. Impact of Small Phonon Energies on the Charge-Carrier Lifetimes in Metal-Halide Perovskites. J. Phys. Chem. Lett. 2018, 9 (5), 939–946.
- (10) Toyozawa, Y. Multiphonon Recombination Processes. Solid-State Electron. 1978, 21 (11–12), 1313–1318.
- (11) Momma, K.; Izumi, F. VESTA 3 for three-dimensional visualization of crystal, volumetric and morphology data. *J. Appl. Crystallogr.* **2011**, 44, 1272–1276.
- (12) Mashiyama, H.; Kawamura, Y.; Kubota, Y. The Anti-Polar Structure of CH3NH3PbBr3. J. Korean Phys. Soc. 2007, 51 (92), 850.
- (13) Brennan, M. C.; Kuno, M.; Rouvimov, S. Crystal Structure of Individual CsPbBr<sub>3</sub> Perovskite Nanocubes. *Inorg. Chem.* **2019**, 58 (2), 1555–1560.
- (14) Cherrette, V. L.; Babbe, F.; Cooper, J. K.; Zhang, J. Z. Octahedral Distortions Generate a Thermally Activated Phonon-Assisted Radiative Recombination Pathway in Cubic CsPbBr <sub>3</sub> Perovskite Quantum Dots. *J. Phys. Chem. Lett.* **2023**, *14* (39), 8717–8725.
- (15) Manser, J. S.; Christians, J. A.; Kamat, P. V. Intriguing Optoelectronic Properties of Metal Halide Perovskites. *Chem. Rev.* **2016**, *116* (21), 12956–13008.
- (16) Fu, J.; Xu, Q.; Han, G.; Wu, B.; Huan, C. H. A.; Leek, M. L.; Sum, T. C. Hot Carrier Cooling Mechanisms in Halide Perovskites. *Nat. Commun.* **2017**, 8 (1), 1300.
- (17) Roberti, T. W.; Cherepy, N. J.; Zhang, J. Z. Nature of the Power-Dependent Ultrafast Relaxation Process of Photoexcited Charge Carriers in II-VI Semiconductor Quantum Dots: Effects of Particle Size, Surface, and Electronic Structure. *J. Chem. Phys.* **1998**, 108 (5), 2143–2151.
- (18) Wheeler, D. A.; Fitzmorris, B. C.; Zhao, H.; Ma, D.; Zhang, J. Ultrafast Exciton Relaxation Dynamics of PbS and Core/Shell PbS/CdS Quantum Dots. *Sci. China Chem.* **2011**, 54 (12), 2009–2015.
- (19) Zhang, J. Z. Optical Properties and Spectroscopy of Nanomaterials; World Scientific: Hackensack, NJ, 2009.
- (20) Zhang, H.; Zeitz, D. C.; Zhang, J. Z. Ultrafast Study of Excited State Dynamics of Amino Metal Halide Molecular Clusters. *J. Phys. Chem. Lett.* **2023**, *14* (36), 8095–8099.
- (21) Mondal, N.; Samanta, A. Complete Ultrafast Charge Carrier Dynamics in Photo-Excited All-Inorganic Perovskite Nanocrystals (CsPbX<sub>3</sub>). *Nanoscale* **2017**, *9* (5), 1878–1885.
- (22) Sheng, C.; Zhang, C.; Zhai, Y.; Mielczarek, K.; Wang, W.; Ma, W.; Zakhidov, A.; Vardeny, Z. V. Exciton versus Free Carrier Photogeneration in Organometal Trihalide Perovskites Probed by Broadband Ultrafast Polarization Memory Dynamics. *Phys. Rev. Lett.* **2015**, *114* (11), No. 116601.
- (23) Pu, Y.-C.; Kibria, M. G.; Mi, Z.; Zhang, J. Z. Ultrafast Exciton Dynamics in InGaN/GaN and Rh/Cr  $_2$  O  $_3$  Nanoparticle-Decorated InGaN/GaN Nanowires. *J. Phys. Chem. Lett.* **2015**, *6* (13), 2649–2656.